Low Energy Phases of Bi Monolayer Predicted by Structure Search in Two Dimensions

Sobhit Singh,[*,†,‡] Zeila Zanolli,[¶,§] Maximilian Amsler,[‖] Brahim Belhadji,[⊥] Jorge O. Sofo,[#] Matthieu J. Verstraete,[⊥,¶] and Aldo H. Romero[*,†]

†*Department of Physics and Astronomy, West Virginia University, Morgantown, WV 26505, USA*

‡*Department of Physics and Astronomy, Rutgers University, Piscataway, NJ 08854, USA*

¶*Catalan Institute of Nanoscience and Nanotechnology (ICN2) and European Theoretical Spectroscopy Facility, CSIC and BIST, Campus UAB, Bellaterra, 08193 Barcelona, Spain*

§*Institute for Theoretical Solid State Physics, RWTH Aachen University, D-52056 Aachen, Germany*

‖*Laboratory of Atomic and Solid State Physics, Cornell University, Ithaca, New York 14853, USA*

⊥*NanoMat/Q-Mat/CESAM and European Theoretical Spectroscopy Facility, Université de Liège (B5), B-4000 Liège, Belgium*

#*The Pennsylvania State University, 201 Old Main, University Park, Pennsylvania 16802, USA*

E-mail: sobhit.singh@rutgers.edu; Aldo.Romero@mail.wvu.edu

Abstract

We employ an *ab-initio* structure search algorithm to explore the configurational space of bismuth in quasi-two dimensions. A confinement potential is introduced to restrict the movement of atoms within a pre-defined thickness to find the stable and metastable forms of monolayer Bi. In addition to the two known low-energy structures (puckered monoclinic and buckled hexagonal), our calculations predict three new phases: α, β, and γ. Each phase exhibits peculiar electronic properties, ranging from metallic (α and γ) to semiconducting (puckered monoclinic, buckled hexagonal, and β). Topologically non trivial features are predicted for buckled hexagonal and γ phases. We also remark on the role of $5d$ electrons on the electronic properties of Bi monolayer. We conclude that Bi provides a rich playground to study distortion-mediated metal-insulator phase transitions in quasi-2D.

Graphical TOC Entry

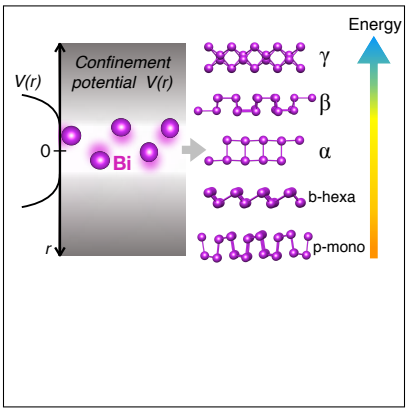

Keywords

Bismuth, structure search, two-dimensional materials, van Hove singularity, topological materials, minima hopping method.

Two dimensional (2D) materials made from group V elements of the periodic table (pnictogens = N, P, As, Sb, Bi) have attracted much attention due to their unique electronic and topological properties.[1–9] Experimental synthesis of phosphorene (a single layer of black phosphorus), which was the first addition to the elemental 2D material family after graphene, has further spurred research into group V elemental 2D materials.[10–12] Recent theoretical predictions as well as the experimental studies revealed the existence of stable 2D nitrogene, arsenene, antimonene, and bismuthene.[2,3,5–8,13–19] Among the pnictogens, Bi is particularly interesting due to its strong intrinsic spin-orbit coupling (SOC) and thermoelectric properties. Large Rashba effect and non-trivial topological phases have been observed in Bi thin films.[20–27] Recently, Reis *et al.* reported the presence of quantum spin Hall effects together with a large energy bandgap (∼0.8 eV) in honeycomb Bi films grown on SiC(0001),[28] thus, making Bi films a potential candidate for the high-temperature quantum spin Hall material. Bi also shows enhanced thermoelectricity in reduced dimensions.[29,30]

The geometric structure of bulk Bi is based on a trigonal pyramid (R-3m space group). The outermost shell of Bi atom has $6s^2 6p^3$ electronic configuration and it tends to form three covalent bonds with neighboring atoms to complete its shell. Hence, Bi atomic layers are naturally expected to have a buckled hexagonal structure. However, recent experiments and theoretical studies suggest that below 4 atomic monolayer thickness Bi prefers a puckered monoclinic structure, similar to phosphorene.[27,31–33] Moreover, a single atomic sheet of Bi contains out-of-plane dangling bonds. These dangling bonds mutually saturate in a two atomic layers stacking. Hence, even numbers of Bi layers are energetically more favorable than the odd ones.[27] The aforementioned two facts, (i) dangling bonds and (ii) two atomic layer stacking, yield a puckered monoclinic phase of monolayer Bi that has been experimentally synthesized on various substrates.[27,31–33] However, depending upon the growth conditions and choice of substrate, Bi atoms could also acquire distinct structural arrangements in the 2D limit, which is yet puzzling.[34,35] Therefore, it is important to understand the energetics of different stable and metastable structures of Bi in quasi-two dimensions.

Here, the first-principles structural search calculations could provide useful information regarding the potential energy landscape and relative energetic stability of different phases of Bi in quasi-2D limit. Although, many global optimization methods have been developed to perform structure search calculations for bulk materials,[36–45] a few have been developed, specifically, to carry out structural search in two dimensions.[46–54] In recent years, several databases have been deployed for 2D materials.[55–61] However, these databases contain principally known 2D materials and/or derivatives of the known 3D ones.

In the present work, we systematically explore the multidimensional potential energy landscape of two atomic layers thick monolayer Bi, using a constrained minima hopping method (cMHM). We predict three new phases (α, β, and γ), in addition to recovering the two known phases of monolayer Bi: puckered monoclinic (p-mono) and buckled hexagonal (b-hexa). Our calculations predict the p-mono phase as the ground state of monolayer Bi, which is consistent with the previous studies.[16,27,31,62] The b-hexa, α, β, and γ phases of monolayer Bi are metastable (listed here in the increasing order of energy). The formation energy comparison of the cMHM predicted phases with an already synthesized graphene-like Bi monolayer phase (on SiC substrate)[28] reveals that the predicted phases are considerably lower in energy, and hence, these structures are within the reach of experimental synthesis. In their free standing form, the p-mono, b-hexa, and β phases are dynamically stable and semiconducting, whereas the metallic α and γ phases exhibit imaginary phonon frequencies implying dynamical instability. We demonstrate that the γ-phase, which hosts a topologically non-trivial Dirac nodal line, can be dynamically stabilized by tensile bi-axial strain and the α-phase can be stabilized under the effect of epitaxy on a substrate. We also discuss the structural, electronic, and vibrational properties of all the obtained low-energy structures in detail, and provide a comprehensive description of the employed 2D structure search method.

Figure 1 shows the optimized crystal structures and formation energies of the five low-energy configurations of monolayer Bi predicted by the cMHM. We also compare the energetics of the predicted low-energy structures with that of a flattened hexagonal Bi monolayer

(f-hexa), which has been recently synthesized on a SiC(0001) substrate.[28] Our cMHM calculations recover the reported p-mono as the ground state, and the b-hexa phase as the first metastable structure.[16,27,31,62] In addition, we predict three new phases of monolayer Bi, which are 63, 72, and 83 meV/atom higher in energy with respect to the lowest energy p-mono phase. Generally, group V elements (N, P, As, Sb, Bi) tend to form a puckered structure in 2 D. Although bulk Bi prefers a rhombohedral structure with alternate stacking of hexagonal buckled Bi monolayers, the b-hexa monolayer is energetically less favorable compared to the p-mono phase by 36 meV/atom.

Table 1: Number of atoms per unit cell (n_{mono}), lattice parameters, cell angles, bond lengths, buckling height (h), formation energy (E_{form}), and relative formation energy ($\Delta\mathrm{E}_{form}$) with respect to the p-mono phase

Structure	n_{mono}	lattice parameters a, b (Å)	cell angles α, β, γ (degrees)	bond length (Å)	h (Å)	E_{form} (meV/atom)	$\Delta\mathrm{E}_{form}$ (meV/atom)
p-mono	8	6.722, 6.722	90, 90, 94	$d = 3.11$	3.10	106	0
b-hexa	2	4.598, 4.598	90, 90, 120	$d = 3.12$	1.63	142	36
α-phase	4	3.561, 5.778	90.7, 89.4, 86.7	$d_1 = 3.30, d_2 = 3.48$	3.16	169	63
β-phase	8	7.955, 7.945	90, 90, 65.9	$d_1 = 3.05, d_2 = 3.15$	2.14	178	72
γ-phase	8	7.613, 7.613	90, 90, 74.1	$d_1 = 3.10, d_2 = 3.31$	2.08	190	83
f-hexa	2	5.329, 5.329	90, 90, 120	$d = 3.08$	0.00	422	316

Crystallographic details and formation energy (E_{form}) of the studied phases are summarized in Table 1. The optimized monolayer structures are provided in the supplemental material (SM).[63] We calculate E_{form} using the formula, $E_{form} = \frac{E_{mono}}{n_{mono}} - \frac{E_{bulk}}{n_{bulk}}$, where E_{mono} (n_{mono}) and E_{bulk} (n_{bulk}) represent the total energy (number of atoms/cell) of the monolayer and bulk Bi (R-3m), respectively. The formation energy also gives us an estimate of the interlayer strength in layered structures. For most of the synthesized single-layer transition-metal dichalcogenides (TMDs), E_{form} ranges from 80 – 150 meV/atom,[64] and for the hexagonal group III–V single layer materials E_{form} ranges from 380 – 520 meV/atom.[65] For comparison, we compute the E_{form} of a Bi monolayer in graphene-like flat hexagonal setting (f-hexa phase), which has recently been synthesized on a SiC substrate.[28] As one would expect for a fully planar honeycomb Bi monolayer, the f-hexa phase has a much

higher formation energy, 316 meV/atom above the p-mono phase. Therefore, we expect that all the cMHM predicted structures are within the reach of experimental synthesis.

In order to test the dynamical stability of the different phases, we calculate their phonon dispersion in 2D Brillouin zone (BZ), as shown in Fig. 2. We find that the p-mono (Fig. 2a), b-hexa (Fig. 2b), and β (Fig. 2c) phases are dynamically stable. The very small dynamical instabilities visible near the Γ point are purely numerical and linked to the 2D out-of-plane acoustic mode (ZA) with quadratic dispersion, which is not perfectly reproduced for $k \to 0$.[9,66] The quadratic dispersion of the ZA phonon mode usually becomes linear in k under strain.[67]

The instability of α and γ phases (see Fig. 2(d, e)) is not surprising as these phases are associated with highly symmetric buckled rectangular-like lattices (Fig. 1): Bi has three valence orbitals (p_x, p_y, p_z), and should form three covalent bonds to saturate its valency. This requirement is met in p-mono, b-hexa and β phases of monolayer Bi, but not in the α and γ phases, where the coordination number is four for each Bi atom. Consequently, the phases will be metallic and a structural instability is expected for the α and γ phases at ambient conditions. However, structures with anomalous coordination numbers can be stabilized under pressure or strain conditions:[68–70] A small structural distortion or charge instability can change the coordination of Bi atoms, and lead to a structural phase transition into one of the lower symmetry phases of monolayer Bi. Deposition on a suitable substrate can also stabilize the unstable phases, as demonstrated in Ref.[28] for f-hexa phase. The f-hexa phase exhibits an unstable phonon mode at the M-point of BZ (Fig. 2f). The stabilization of the unstable ZA acoustic mode at the M-point yields puckering in the f-hexa phase. However, upon deposition on a SiC substrate, Bi atoms bind to the substrate and stabilize this phase.

Strain can make γ-phase dynamically stable, as this phase does not exhibit any unstable phonon mode at the high-symmetry points of BZ. In fact, we find that a tensile bi-axial strain of 8 % stabilizes the phonons in γ phase (see SM[63]). Deposition on a substrate, instead, might stabilize α-phase due to the the presence of large imaginary phonon frequencies

at the S-point $(\frac{1}{2}, \frac{1}{2})$ of BZ. A list of potential substrates for epitaxial fabrication of α-phase is given in the SM,[63] where we report structures with the lowest strain obtained by performing a search over the Open Quantum Materials Database (OQMD).[71] The monolayer/substrate matching search was performed by imposing a maximum difference in strain of 5%, a maximum area of 40 Å^2, and a maximum angle difference of 1°. The search was performed using the implementation discussed in Ref.[72] Study of the substrate effects on the studied monolayer phases is beyond the scope of present work.

Each of the predicted structures presents very specific electronic properties, as illustrated in Figure 3. First-principles calculations with inclusion of SOC show that the p-mono (Fig. 3a), b-hexa (Fig. 3b), f-hexa (Fig. 3f), and β (Fig. 3c) phases are semiconducting, whereas α (Fig. 3d) and γ (Fig. 3e) phases are metallic. Without SOC (see SM[63]), we observe a direct energy bandgap (DFT-PBE) of 0.52, 0.43, and 0.80 eV in p-mono, b-hexa, and β phases, respectively. The strong SOC of bismuth reduces the bandgap of the semiconducting phases to 0.34, 0.08, and 0.14 eV, and changes the direct gap nature of p-mono and β to indirect (transition marked as a red arrow in Fig. 3 (a, c)). The f-hexa phase exhibits two gapless Dirac points near the K point without-SOC (see SM[63]). However, inclusion of SOC opens a wide mass gap at the Dirac points yielding an indirect bandgap of 0.51 eV near the K-point, which is in agreement with data reported in Ref.[28] The SOC induces a spin-splitting of electronic bands in the non-centrosymmetric p-mono and β phases. No SOC-induced spin-splitting occurs in the b-hexa, f-hexa, and γ phases due to the protected inversion-symmetry. However, the top valence band in b-hexa inherits a Mexican-hat type dispersion near the Γ point (inset of Fig. 3b) which leads to a van Hove singularity in the density of states near the Fermi-level (E_F),[73,74] as discussed later. This is particularly interesting because a small amount of charge doping (hole doping) will trigger time-reversal symmetry breaking and may give rise to emergent phenomena such as ferromagnetism, ferroelasticity, multiferroicity, or superconductivity in two dimensions.[73]

We remark that the structural and electronic properties obtained for b-hexa differ from

those reported by Aktürk *et al.*[16] due to the explicit inclusion of semicore $5d^{10}$ electrons in the pseudopotential used in our calculations. Considering the Bi $5d$ states in the core, the bandgap predicted in Ref.[16] is 0.547 eV, much larger than our 0.08 eV, and the optimized lattice parameters are 4.38 Å, perceptibly smaller than our 4.598 Å. The bandgap reduction is due to a lifting of the p-orbital degenerate crossing at Γ, pushing the top valence band higher in energy. The shift results from the crystal field splitting of the d electrons (absent in the pseudopotential's frozen core) and their symmetry-breaking effect on the dangling bond orbitals in the last two valence bands. In the SM[63] we show that by keeping Bi $5d$ electrons in the core we can replicate the results of Ref.[16] Calculations with explicit d electrons produce more accurate results, as has been reported for bulk Bi.[75,76] As a final check, we have used the all-electron ELK code[77] to calculate the electronic band structure, and it agrees fully with the results including d electrons in the valence (see SM[63]).

Our calculations for f-hexa monolayer, in which no crystal field splitting effects are expected, reveal negligible difference in the electronic bandstructure calculated with and without inclusion of Bi $5d$ electrons in the core.[63] We note that the p-orbital splitting in b-hexa due to the semi-core d is a considerable but quite subtle effect, and none of the other phases are as sensitive to $5d$ states as the b-hexa phase. For p-mono phase, PBE+SOC predicted bandgap changes only from 0.34 eV to 0.39 eV upon freezing the Bi $5d^{10}$ electrons in the core.

Valley spin-splitting effects are observed in the electronic band structure of the dynamically stable β-phase along the Γ-X and Γ-Y directions. Figure 4 shows the spin-projected electronic band structure of β-phase calculated with-SOC along $-X \rightarrow \Gamma \rightarrow X$ and $-Y \rightarrow \Gamma \rightarrow Y$ directions. The spin polarization is entirely contained in the $x-y$ plane, with two valleys polarized along $-x+y$ and the other two polarized along $+x-y$ due to the C_2 rotational symmetry. The conduction and valence band edges have opposite spin polarization in both directions. The two lowest conduction and two highest valence bands are all composed of p_z orbitals. The dispersion and spin-texture of the lowest conduction

band and two highest valence bands in Fig. 4 resemble the electronic band structure of single layer transition metal dichalcogenides MX_2 ($M = \{Mo, W\}$, and $X = \{S, Se\}$), in which spin-valley effects have been observed.[78–81] The broken inversion-symmetry and strong SOC effects lift the spin degeneracy of bands everywhere except at the Kramer's points of the β-phase. The time-reversal symmetry further couples the spin and valley degrees of freedom of valleys located at $\pm\mathbf{k}$, yielding valley-specific optical selection rules. This is similar to the case of MX_2 monolayers,[78,79,81,82] but with in-plane instead of the out-of-plane spin texture, which may yield novel spin-pseudospin and magnetic valley couplings. The corresponding optical transitions can be probed in photoluminescence measurements using circularly polarized light.

In γ-phase, we observe signatures of interesting topological Lifshitz transitions with changes in the chemical potential near the Fermi-level (see SM[63]). This suggests the occurrence of distinct topological phase transitions in the γ phase.[83] Strikingly, we find that the γ phase hosts topologically protected gapless type-I Dirac points (DPs) near the Fermi-level, as shown in Fig. 3e along $\Gamma \to X$ and $\Gamma \to Y$ paths. The DPs result from an inverted band-ordering of p_z (conduction) and $p_{x,y}$ (valence) bands near the Γ point (Fig. 5). Since these bands belong to different 1 D irreducible representations, they are allowed to cross along the high-symmetry line, and these band-crossings near the Fermi-level are topologically protected by the mirror symmetries of the monolayer. The direct coordinates of DPs, residing at energies E_F−0.025 eV, in momentum space are (±0.167, 0, 0) and (0, ±0.167, 0). These points belong to a Dirac nodal line centered at the Γ point, as shown in the SM.[63]

In order to further verify the nontrivial topological nature of γ-phase, we compute the Z_2 topological invariant using the Fu-Kane parity approach.[84] Our results indicate that γ-phase is a strong topological insulator (technically, a Dirac semimetal) with $Z_2 = 1$ owing to a band-inversion at Γ point. The nontrivial topological features of γ-phase are also visible in the edge states calculations shown in the SM.[63] We also compute the Z_2 topological invariant for inversion-symmetric b-hexa and f-hexa phases, and obtain that b-hexa phase belong to a

topological nontrivial class with $Z_2 = 1$, whereas the f-hexa phase belongs to a topological trivial class with $Z_2 = 0$ (details in SM[63]). This indicates that the reported topological phase in the f-hexa phase is induced by substrate proximity, as suggested by Reis et al.[28] In presence of a substrate, the Bi-p_z electrons, which are unsaturated in an isolated f-hexa monolayer, saturate by hybridizing with the substrate orbitals, thus, leading to a nontrivial topological phase in the monolayer/substrate heterosystem.

The orbital projected density of states (DOS) for all phases are provided in the SM.[63] The DOS plots confirm the semiconducting behavior of p-mono, b-hexa, f-hexa, and β phases, and metallic behavior of the α and γ phases. Notably, we observe a sharp enhancement in the DOS of b-hexa phase at the Fermi-level (Fig. 6), which originates due to the Mexican-hat type shape of the highest valence band near the Γ point and is signature of van Hove singularity. Such a divergence in the DOS can lead to an electronic instability, often resulting in structural distortions, magnetism, or superconductivity at specific conditions.[73] Here, we note that this feature is also visible in the edge state spectrum of the b-hexa phase (see SM[63]). Finally, we list the estimated bandgap values, obtained using the PBE and HSE06 approximations, in Table 2.

Table 2: Energy bandgap (eV units) estimated from the PBE and HSE06 approximations

		p-mono	b-hexa	α	β	γ	f-hexa
PBE	with-SOC	0.34	0.08	metal	0.14	semimetal	0.51
	without-SOC	0.52	0.43	metal	0.80	semimetal	semimetal
HSE06	with-SOC	0.13	0.12	metal	0.47	semimetal	0.40
	without-SOC	0.51	0.72	metal	1.16	semimetal	semimetal

In summary, we study five low-energy phases of monolayer Bi that are obtained from a systematic structural search in quasi-two dimensions along with an already synthesized f-hexa phase.[28] These phases reveal the multifunctional behaviour of Bi in quasi-2 D. In the lowest energy phase, Bi atoms prefer a puckered monoclinic structure instead of a hexagonal buckled structure. In terms of the formation energy, the studied phases rank (from low to

high) as follows: p-mono, b-hexa, α, β, γ, and f-hexa. The p-mono, b-hexa, and β phases are dynamically stable, whereas the α and γ phases can be stabilized under the effect of substrate epitaxy and strain. We find that the p-mono, b-hexa, β, and f-hexa phases are semiconducting, whereas the α and γ phases exhibit metallic properties. Interestingly, we notice the signatures of the van Hove singularity in the buckled hexagonal phase. Topological nontrivial features are observed in the electronic spectrum of the b-hexa and γ phases. The γ phase hosts a topological Dirac nodal line together with the signatures of intriguing topological Lifshitz transitions occurring near the Fermi-level. Our results suggest that the reported[28] topological phase in the f-hexa phase is not intrinsic, rather it is induced by the substrate proximity. We further comment on the essential role of semicore Bi-5d electrons in the determination of electronic bandstructure near the Fermi-level. A structural distortion-mediated metal-insulator phase transition can be realized in the reported Bi monolayers.

METHODS

Structure search algorithm:– The computational prediction of new structures for a given atomic composition requires a systematic exploration of the multidimensional potential energy surface (PES), in order to find the global and local minima. In this work, we employ the minima hopping method (MHM[85,86]) to carry out structural search calculations. This method seeks local minima on the multidimensional PES, using an efficient dynamical algorithm, combining Density Functional Theory (DFT) to evaluate energy and forces, and short Molecular Dynamics (MD) simulations to help escape from a local minimum and explore new regions of the PES. The initial velocities during MD simulations are aligned along the soft mode direction to cross over low-energy barriers, thereby exploiting the Bell-Evans-Polanyi principle.[87,88] The MHM employs a feedback mechanism to avoid revisiting local minima and to accelerate the search. More details of this method for structure search in 3D can be found in Refs.,[75,89–91] and the technical details for structure search in 2D are given below.

In order to perform structure searches in two dimensions, we add a confinement potential, to restrict the motion of atoms within a pre-defined thickness. Within this region, the confinement potential is very weak compared to electronic energy levels, but it increases quartically outside this pre-defined thickness, similar to a particle in a well problem. Thus, the search is restricted to find the low-energy arrangements of atoms in a constrained quasi-2D space. This approach has been successfully applied to identify two-dimensional forms of TiO_2.[53] A two-dimensional confining potential $C(e, \mathbf{r}_i^\alpha)$ is added to the target energy function to be optimized, where α denotes the axis $\alpha = \{x, y, z\}$ along the non-periodic direction, $\mathbf{r}_i$ are the Cartesian coordinates of the N atoms in the system, and e is the equilibrium positions along α at which the potential is centered. As the confinement function we use a C with piece-wise continuous derivative, which is zero within a cutoff region r_c around e, while it has a polynomial form of order n and amplitude A beyond r_c:

$$C^\alpha = \sum_{i=1}^{N} c(e, \mathbf{r}_i^\alpha) \tag{1}$$

where,

$$c(e, \mathbf{r}_i^\alpha) = \begin{cases} A(|e - \mathbf{r}_i^\alpha| - r_c)^n, & \text{for } |e - \mathbf{r}_i^\alpha| \geq r_c \\ 0, & \text{otherwise} \end{cases} \tag{2}$$

The derivatives with respect to the atomic coordinates $\mathbf{f}_i = \frac{\partial C_i}{\partial \mathbf{r}_i}$ and the cell vectors $\sigma_i = \frac{\partial C}{\partial h_i}$ were taken fully into account during the local geometry optimizations, the MD escape trials, and for aligning the initial MD velocities along the soft mode directions, a process that we call softening. Note that the above atomic positions are expressed in the reduced coordinates $\mathbf{r}_i = h\mathbf{s}_i$, and $h = (\mathbf{a}, \mathbf{b}, \mathbf{c})$ is the matrix containing the lattice vectors. In our structural search runs we used a confinement potential centered along the lattice vector $\mathbf{c}$ (*i.e.* $\alpha = z$), with a cutoff $r_c = 0.3$ Å, $n = 4$ and $A = 0.1$ eV. Confinement was employed for the MD part, whereas DFT relaxation of atoms was completely free from any constraint, allowing the thickness of monolayer to be larger than r_c. We considered 4, 8, 12,

and 16 atoms per unit cell in our structure search calculations. A total of 98, 51, 36, and 81 minima were found for 4, 8, 12, and 16 atoms/cell, respectively. The obtained minima were further re-optimized using a tighter convergence criteria of k-mesh sampling and energy cutoff for the plane wave basis set.

Ab-initio calculations:– Density Functional Theory (DFT) based first-principles calculations were carried out using Projector Augmented Wave (PAW) method as implemented in the VASP software.[92] We considered fifteen valence electrons of Bi ($5d^{10}6s^26p^3$) in the PAW pseudo-potential. The exchange-correlation energy was computed within the generalized gradient approximation using the PBE exchange-correlation functional as parametrized by Perdew-Burke-Ernzerhof.[93] SOC was included self-consistently. We used 600 eV as the kinetic energy cutoff of the plane wave basis set and a $11 \times 11 \times 1$ Monkhorst-Pack k-mesh was used to sample the reciprocal space for structural optimization. The electronic density of states (DOS) was calculated using a k-mesh of size $21 \times 21 \times 1$. We used a Γ-type sampling scheme for hexagonal structure and Monkhorst-Pack scheme was used to sample the Brillouin zone of all other structures. Structural relaxations were performed until all the atomic forces were less than 10^{-3} eV/Å, and 10^{-8} eV was used as the energy convergence criterion for self-consistent DFT calculations. Phonon calculations (with-SOC) were performed using the finite-displacement approach, and the PHONOPY software[94] was used to evaluate the force constants. Depending upon the size of unit cell, supercells of size $3 \times 3 \times 1$ or $4 \times 4 \times 1$ were used for phonon calculations. A vacuum of thickness larger than 14 Å was added to avoid any periodic interaction between two adjacent Bi monolayers. The PYPROCAR code was used to analyze the electronic band structures and spin-textures. The WannierTools package[95] was used to analyze the topological properties.

Acknowledgments

The authors are grateful to Sangeeta Sharma and Kay Dewhurst for their assistance with the ELK code. We also acknowledge the support by Pedram Tavazohi on the substrate search candidates for epitaxial growth. This work used the Extreme Science and Engineering Discovery Environment (XSEDE), which is supported by National Science Foundation grant number OCI-1053575. Additionally, the authors acknowledge support from Texas Advances Computer Center (TACC), Bridges supercomputer at Pittsburgh Supercomputer Center and Super Computing Systems (Spruce and Mountaineer) at West Virginia University (WVU). AHR and SS acknowledge support from National Science Foundation (NSF) DMREF-NSF 1434897, NSF OAC-1740111, and DOE DE-SC0016176 projects. SS acknowledges support from the Dr. Mohindar S. Seehra Research Award and the Distinguished Doctoral Scholarship at West Virginia University. ZZ acknowledges financial support by the Ramon y Cajal program (RYC-2016-19344), the CERCA programme of the Generalitat de Catalunya (grant 2017SGR1506), the Severo Ochoa programme (MINECO, SEV-2017-0706), and the Deutsche Forschungsgemeinschaft (DFG) Grant No. ZA 780/3-1. MA acknowledges support from the Novartis Universität Basel Excellence Scholarship for Life Sciences and the Swiss National Science Foundation (Project No. P300P2-158407, P300P2-174475). MJV acknowledges ULiege and FNRS for a sabbatical grant at ICN2 (2018-2019).

Supplemental Information Available

Supplemental Material contains details related to the role of semicore Bi-5d electrons on the electronic bandstructure of monolayer Bi, DFT optimized structures, electronic bandstructure calculated without SOC, strain-stabilized phonon spectrum of γ phase, topological characterization, atomic orbitals resolved electronic bandstructure for f-hexa and γ phases, spin-textures calculated at constant energy surfaces for γ phase, potential substrates for α phase, and calculated density of states for all studied phases.

Authors Information

Corresponding Authors

Sobhit Singh: sobhit.singh@rutgers.edu

Aldo H. Romero: Aldo.Romero@mail.wvu.edu

ORCID iD

Sobhit Singh: 0000-0002-5292-4235

Zeila Zanolli: 0000-0003-0860-600X

Maximilian Amsler: 0000-0001-8350-2476

Jorge O. Sofo: 0000-0003-4513-3694

Matthieu J. Verstraete: 0000-0001-6921-5163

Aldo H. Romero: 0000-0001-5968-0571

References

(1) Butler, S. Z.; Hollen, S. M.; Cao, L.; Cui, Y.; Gupta, J. A.; Gutiérrez, H. R.; Heinz, T. F.; Hong, S. S.; Huang, J.; Ismach, A. F. et al. Progress, Challenges, and Opportunities in Two-Dimensional Materials Beyond Graphene. *ACS Nano* **2013**, *7*, 2898–2926.

(2) Zhu, Z.; Tománek, D. Semiconducting Layered Blue Phosphorus: A Computational Study. *Phys. Rev. Lett.* **2014**, *112*, 176802.

(3) Rivero, P.; Yan, J.-A.; García-Suárez, V. M.; Ferrer, J.; Barraza-Lopez, S. Stability and properties of high-buckled two-dimensional tin and lead. *Phys. Rev. B* **2014**, *90*, 241408.

(4) Miró, P.; Audiffred, M.; Heine, T. An atlas of two-dimensional materials. *Chem. Soc. Rev.* **2014**, *43*, 6537–6554.

(5) Özçelik, V. O.; Aktürk, O. U.; Durgun, E.; Ciraci, S. Prediction of a two-dimensional crystalline structure of nitrogen atoms. *Phys. Rev. B* **2015**, *92*, 125420.

(6) Wu, Q.; Shen, L.; Yang, M.; Cai, Y.; Huang, Z.; Feng, Y. P. Electronic and transport properties of phosphorene nanoribbons. *Phys. Rev. B* **2015**, *92*, 035436.

(7) Kou, L.; Chen, C.; Smith, S. C. Phosphorene: Fabrication, Properties, and Applications. *The Journal of Physical Chemistry Letters* **2015**, *6*, 2794–2805.

(8) Balendhran, S.; Walia, S.; Nili, H.; Sriram, S.; Bhaskaran, M. Elemental analogues of graphene: silicene, germanene, stanene, and phosphorene. *Small* **2015**, *11*, 640–652.

(9) Singh, S.; Romero, A. H. Giant tunable Rashba spin splitting in a two-dimensional BiSb monolayer and in BiSb/AlN heterostructures. *Phys. Rev. B* **2017**, *95*, 165444.

(10) Liu, H.; Neal, A. T.; Zhu, Z.; Luo, Z.; Xu, X.; Tománek, D.; Ye, P. D. Phosphorene: An Unexplored 2D Semiconductor with a High Hole Mobility. *ACS Nano* **2014**, *8*, 4033–4041.

(11) Li, L.; Yu, Y.; Ye, G. J.; Ge, Q.; Ou, X.; Wu, H.; Feng, D.; Chen, X. H.; Zhang, Y. Black phosphorus field-effect transistors. *Nature Nanotechnology* **2014**, *9*, 372–377.

(12) Churchill, H. O. H.; Jarillo-Herrero, P. Phosphorus joins the family. *Nature Nanotechnology* **2014**, *9*, 330–331.

(13) Liu, H.; Neal, A. T.; Zhu, Z.; Luo, Z.; Xu, X.; Tománek, D.; Ye, P. D. Phosphorene: An Unexplored 2D Semiconductor with a High Hole Mobility. *ACS Nano* **2014**, *8*, 4033–4041.

(14) Kamal, C.; Ezawa, M. Arsenene: Two-dimensional buckled and puckered honeycomb arsenic systems. *Phys. Rev. B* **2015**, *91*, 085423.

(15) Özçelik, V. O.; Aktürk, O. U.; Durgun, E.; Ciraci, S. Prediction of a two-dimensional crystalline structure of nitrogen atoms. *Phys. Rev. B* **2015**, *92*, 125420.

(16) Aktürk, E.; Aktürk, O. U.; Ciraci, S. Single and bilayer bismuthene: Stability at high temperature and mechanical and electronic properties. *Phys. Rev. B* **2016**, *94*, 014115.

(17) Ersan, F.; Aktürk, E.; Ciraci, S. Stable single-layer structure of group-V elements. *Phys. Rev. B* **2016**, *94*, 245417.

(18) Zhang, Q.; Schwingenschlögl, U. Emergence of Dirac and quantum spin Hall states in fluorinated monolayer As and AsSb. *Phys. Rev. B* **2016**, *93*, 045312.

(19) Pumera, M.; Sofer, Z. 2D Monoelemental Arsenene, Antimonene, and Bismuthene: Beyond Black Phosphorus. *Advanced Materials* **2017**, *29*, 1605299.

(20) Koroteev, Y. M.; Bihlmayer, G.; Gayone, J. E.; Chulkov, E. V.; Blügel, S.; Echenique, P. M.; Hofmann, P. Strong Spin-Orbit Splitting on Bi Surfaces. *Phys. Rev. Lett.* **2004**, *93*, 046403.

(21) Hirahara, T.; Nagao, T.; Matsuda, I.; Bihlmayer, G.; Chulkov, E. V.; Koroteev, Y. M.; Echenique, P. M.; Saito, M.; Hasegawa, S. Role of Spin-Orbit Coupling and Hybridization Effects in the Electronic Structure of Ultrathin Bi Films. *Phys. Rev. Lett.* **2006**, *97*, 146803.

(22) Ast, C. R.; Henk, J.; Ernst, A.; Moreschini, L.; Falub, M. C.; Pacilé, D.; Bruno, P.; Kern, K.; Grioni, M. Giant Spin Splitting through Surface Alloying. *Phys. Rev. Lett.* **2007**, *98*, 186807.

(23) Koroteev, Y. M.; Bihlmayer, G.; Chulkov, E. V.; Blügel, S. First-principles investigation of structural and electronic properties of ultrathin Bi films. *Phys. Rev. B* **2008**, *77*, 045428.

(24) Kim, H.-J.; Cho, J.-H. Giant spin-orbit-induced spin splitting in Bi zigzag chains on GaAs(110). *Phys. Rev. B* **2015**, *92*, 085303.

(25) Ma, Y.; Li, X.; Kou, L.; Yan, B.; Niu, C.; Dai, Y.; Heine, T. Two-dimensional inversion-asymmetric topological insulators in functionalized III-Bi bilayers. *Phys. Rev. B* **2015**, *91*, 235306.

(26) Singh, S.; Garcia-Castro, A. C.; Valencia-Jaime, I.; Muñoz, F.; Romero, A. H. Prediction and control of spin polarization in a Weyl semimetallic phase of BiSb. *Phys. Rev. B* **2016**, *94*, 161116.

(27) Lu, Y.; Xu, W.; Zeng, M.; Yao, G.; Shen, L.; Yang, M.; Luo, Z.; Pan, F.; Wu, K.; Das, T. et al. Topological Properties Determined by Atomic Buckling in Self-Assembled Ultrathin Bi(110). *Nano Letters* **2015**, *15*, 80–87.

(28) Reis, F.; Li, G.; Dudy, L.; Bauernfeind, M.; Glass, S.; Hanke, W.; Thomale, R.; Schäfer, J.; Claessen, R. Bismuthene on a SiC substrate: A candidate for a high-temperature quantum spin Hall material. *Science* **2017**, *357*, 287–290.

(29) Heremans, J.; Thrush, C. M. Thermoelectric power of bismuth nanowires. *Phys. Rev. B* **1999**, *59*, 12579–12583.

(30) Dresselhaus, M.; Chen, G.; Tang, M.; Yang, R.; Lee, H.; Wang, D.; Ren, Z.; Fleurial, J.-P.; Gogna, P. New Directions for Low-Dimensional Thermoelectric Materials. *Advanced Materials* **2007**, *19*, 1043–1053.

(31) Nagao, T.; Sadowski, J. T.; Saito, M.; Yaginuma, S.; Fujikawa, Y.; Kogure, T.; Ohno, T.; Hasegawa, Y.; Hasegawa, S.; Sakurai, T. Nanofilm Allotrope and Phase Transformation of Ultrathin Bi Film on Si(111)-7×7. *Phys. Rev. Lett.* **2004**, *93*, 105501.

(32) Scott, S.; Kral, M.; Brown, S. A crystallographic orientation transition and early stage growth characteristics of thin Bi films on HOPG. *Surface Science* **2005**, *587*, 175 – 184.

(33) Fang, A.; Adamo, C.; Jia, S.; Cava, R. J.; Wu, S.-C.; Felser, C.; Kapitulnik, A. Bursting at the seams: Rippled monolayer bismuth on $NbSe_2$. *Science Advances* **2018**, *4*, eaaq0330.

(34) Sharma, H. R.; Fournée, V.; Shimoda, M.; Ross, A. R.; Lograsso, T. A.; Gille, P.; Tsai, A. P. Growth of Bi thin films on quasicrystal surfaces. *Phys. Rev. B* **2008**, *78*, 155416.

(35) Hirahara, T.; Fukui, N.; Shirasawa, T.; Yamada, M.; Aitani, M.; Miyazaki, H.; Matsunami, M.; Kimura, S.; Takahashi, T.; Hasegawa, S. et al. Atomic and Electronic Structure of Ultrathin Bi(111) Films Grown on Bi_2Te_3(111) Substrates: Evidence for a Strain-Induced Topological Phase Transition. *Phys. Rev. Lett.* **2012**, *109*, 227401.

(36) Pickard, C. J.; Needs, R. J. High-Pressure Phases of Silane. *Phys. Rev. Lett.* **2006**, *97*, 045504.

(37) Martoňák, R.; Laio, A.; Parrinello, M. Predicting Crystal Structures: The Parrinello-Rahman Method Revisited. *Phys. Rev. Lett.* **2003**, *90*, 075503.

(38) Pannetier, J.; Bassas-Alsina, J.; Rodriguez-Carvajal, J.; Caignaert, V. Prediction of crystal structures from crystal chemistry rules by simulated annealing. *Nature* **1990**, *346*, 343–345.

(39) Wales, D. J.; Scheraga, H. A. Global Optimization of Clusters, Crystals, and Biomolecules. *Science* **1999**, *285*, 1368–1372.

(40) Zhu, Q.; Oganov, A. R.; Lyakhov, A. O. Evolutionary metadynamics: a novel method to predict crystal structures. *CrystEngComm* **2012**, *14*, 3596–3601.

(41) Bush, T. S.; Catlow, C. R. A.; Battle, P. D. Evolutionary programming techniques for predicting inorganic crystal structures. *J. Mater. Chem.* **1995**, *5*, 1269–1272.

(42) M. Woodley, S.; D. Battle, P.; D. Gale, J.; Richard A. Catlow, C. The prediction of inorganic crystal structures using a genetic algorithm and energy minimisation. *Phys. Chem. Chem. Phys.* **1999**, *1*, 2535–2542.

(43) Oganov, A. R.; Glass, C. W. Crystal structure prediction using ab initio evolutionary techniques: Principles and applications. *The Journal of Chemical Physics* **2006**, *124*, 244704.

(44) Wang, Y.; Lv, J.; Zhu, L.; Ma, Y. Crystal structure prediction via particle-swarm optimization. *Phys. Rev. B* **2010**, *82*, 094116.

(45) Avendano-Franco, G.; Romero, A. H. Firefly Algorithm for Structural Search. *Journal of Chemical Theory and Computation* **2016**, *12*, 3416–3428.

(46) Wang, Y.; Miao, M.; Lv, J.; Zhu, L.; Yin, K.; Liu, H.; Ma, Y. An effective structure prediction method for layered materials based on 2D particle swarm optimization algorithm. *The Journal of Chemical Physics* **2012**, *137*, 224108.

(47) Wu, X.; Dai, J.; Zhao, Y.; Zhuo, Z.; Yang, J.; Zeng, X. C. Two-Dimensional Boron Monolayer Sheets. *ACS Nano* **2012**, *6*, 7443–7453.

(48) Lu, H.; Mu, Y.; Bai, H.; Chen, Q.; Li, S.-D. Binary nature of monolayer boron sheets from ab initio global searches. *The Journal of Chemical Physics* **2013**, *138*, 024701.

(49) Luo, W.; Ma, Y.; Gong, X.; Xiang, H. Prediction of Silicon-Based Layered Structures for Optoelectronic Applications. *Journal of the American Chemical Society* **2014**, *136*, 15992–15997.

(50) Zhao, Y.; Zeng, S.; Ni, J. Superconductivity in two-dimensional boron allotropes. *Phys. Rev. B* **2016**, *93*, 014502.

(51) Zhou, X.-F.; Oganov, A. R.; Wang, Z.; Popov, I. A.; Boldyrev, A. I.; Wang, H.-T. Two-dimensional magnetic boron. *Phys. Rev. B* **2016**, *93*, 085406.

(52) Revard, B. C.; Tipton, W. W.; Yesypenko, A.; Hennig, R. G. Grand-canonical evolutionary algorithm for the prediction of two-dimensional materials. *Phys. Rev. B* **2016**, *93*, 054117.

(53) Eivari, H. A.; Ghasemi, S. A.; Tahmasbi, H.; Rostami, S.; Faraji, S.; Rasoulkhani, R.; Goedecker, S.; Amsler, M. Two-Dimensional Hexagonal Sheet of TiO_2. *Chemistry of Materials* **2017**, *29*, 8594–8603.

(54) Singh, A. K.; Revard, B. C.; Ramanathan, R.; Ashton, M.; Tavazza, F.; Hennig, R. G. Genetic algorithm prediction of two-dimensional group-IV dioxides for dielectrics. *Phys. Rev. B* **2017**, *95*, 155426.

(55) Mounet, N.; Gibertini, M.; Schwaller, P.; Campi, D.; Merkys, A.; Marrazzo, A.; Sohier, T.; Castelli, I. E.; Cepellotti, A.; Pizzi, G. et al. Two-dimensional materials from high-throughput computational exfoliation of experimentally known compounds. *Nature Nanotechnology* **2018**, *13*, 246–252.

(56) Haastrup, S.; Strange, M.; Pandey, M.; Deilmann, T.; Schmidt, P. S.; Hinsche, N. F.; Gjerding, M. N.; Torelli, D.; Larsen, P. M.; Riis-Jensen, A. C. et al. The Computational 2D Materials Database: high-throughput modeling and discovery of atomically thin crystals. *2D Materials* **2018**, *5*, 042002.

(57) Rasmussen, F. A.; Thygesen, K. S. Computational 2D Materials Database: Electronic Structure of Transition-Metal Dichalcogenides and Oxides. *The Journal of Physical Chemistry C* **2015**, *119*, 13169–13183.

(58) Choudhary, K.; Kalish, I.; Beams, R.; Tavazza, F. High-throughput Identification and Characterization of Two-dimensional Materials using Density functional theory. *Scientific Reports* **2017**, *7*, 5179.

(59) Midwest Nano Infrastructure Corridor 2D Database hosted by University of Minnesota, Minneapolis, USA. Available from: http://apps. minic.umn.edu/2D/result.php.

(60) Ashton, M.; Paul, J.; Sinnott, S. B.; Hennig, R. G. Topology-Scaling Identification of Layered Solids and Stable Exfoliated 2D Materials. *Phys. Rev. Lett.* **2017**, *118*, 106101.

(61) Paul, J. T.; Singh, A. K.; Dong, Z.; Zhuang, H.; Revard, B. C.; Rijal, B.; Ashton, M.; Linscheid, A.; Blonsky, M.; Gluhovic, D. et al. Computational methods for 2D materials: discovery, property characterization, and application design. *Journal of Physics: Condensed Matter* **2017**, *29*, 473001.

(62) Zhang, S.; Xie, M.; Li, F.; Yan, Z.; Li, Y.; Kan, E.; Liu, W.; Chen, Z.; Zeng, H. Semiconducting Group 15 Monolayers: A Broad Range of Band Gaps and High Carrier Mobilities. *Angewandte Chemie International Edition* **2016**, *55*, 1666–1669.

(63) Supplemental Material contains information related to the optimized structures, DOS, atomic orbitals resolved electronic bandstructures, spin-textures calculated at constant energy surfaces for the γ phase, topological characterization, role of semicore Bi-5d electrons on the electronic bandstructure, strain-stabilized phonon spectrum of γ phase, and potential substrates for α phase.

(64) Zhuang, H. L.; Hennig, R. G. Computational Search for Single-Layer Transition-Metal Dichalcogenide Photocatalysts. *The Journal of Physical Chemistry C* **2013**, *117*, 20440–20445.

(65) Zhuang, H. L.; Singh, A. K.; Hennig, R. G. Computational discovery of single-layer III-V materials. *Phys. Rev. B* **2013**, *87*, 165415.

(66) Singh, S.; Espejo, C.; Romero, A. H. Structural, electronic, vibrational, and elastic properties of graphene/MoS_2 bilayer heterostructures. *Phys. Rev. B* **2018**, *98*, 155309.

(67) Soni, H.; Jha, P. K. Ab-initio study of dynamical properties of two dimensional MoS_2 under strain. *AIP Advances* **2015**, *5*, 107103.

(68) Takarabe, K. Optical Properties of InS under High Pressure. *physica status solidi (b)* **1988**, *145*, 219–225.

(69) McMillan, P. F. High pressure synthesis of solids. *Current Opinion in Solid State and Materials Science* **1999**, *4*, 171 – 178.

(70) Lapidus, S. H.; Halder, G. J.; Chupas, P. J.; Chapman, K. W. Exploiting High Pressures to Generate Porosity, Polymorphism, And Lattice Expansion in the Nonporous Molecular Framework $Zn(CN)_2$. *Journal of the American Chemical Society* **2013**, *135*, 7621–7628.

(71) Kirklin, S.; Saal, J. E.; Meredig, B.; Thompson, A.; Doak, J. W.; Aykol, M.; Rühl, S.; Wolverton, C. The Open Quantum Materials Database (OQMD): assessing the accuracy of DFT formation energies. *npj Computational Materials* **2015**, *1*, 15010.

(72) Mathew, K.; Singh, A. K.; Gabriel, J. J.; Choudhary, K.; Sinnott, S. B.; Davydov, A. V.; Tavazza, F.; Hennig, R. G. MPInterfaces: A Materials Project based Python tool for high-throughput computational screening of interfacial systems. *Computational Materials Science* **2016**, *122*, 183–190.

(73) Seixas, L.; Rodin, A. S.; Carvalho, A.; Castro Neto, A. H. Multiferroic Two-Dimensional Materials. *Phys. Rev. Lett.* **2016**, *116*, 206803.

(74) Özdamar, B.; Özbal, G.; Ç ınar, M. N. m. c.; Sevim, K.; Kurt, G.; Kaya, B.; Sevinçli, H. Structural, vibrational, and electronic properties of single-layer hexagonal crystals of group IV and V elements. *Phys. Rev. B* **2018**, *98*, 045431.

(75) Singh, S.; Ibarra-Hernandez, W.; Valencia-Jaime, I.; Avendano-Franco, G.;

Romero, A. H. Investigation of novel crystal structures of Bi-Sb binaries predicted using the minima hopping method. *Phys. Chem. Chem. Phys.* **2016**, *18*, 29771–29785.

(76) Singh, S.; Valencia-Jaime, I.; Pavlic, O.; Romero, A. H. Elastic, mechanical, and thermodynamic properties of Bi-Sb binaries: Effect of spin-orbit coupling. *Phys. Rev. B* **2018**, *97*, 054108.

(77) Krieger, K.; Dewhurst, J. K.; Elliott, P.; Sharma, S.; Gross, E. K. U. Laser-Induced Demagnetization at Ultrashort Time Scales: Predictions of TDDFT. *Journal of Chemical Theory and Computation* **2015**, *11*, 4870–4874.

(78) Yao, W.; Xiao, D.; Niu, Q. Valley-dependent optoelectronics from inversion symmetry breaking. *Phys. Rev. B* **2008**, *77*, 235406.

(79) Sallen, G.; Bouet, L.; Marie, X.; Wang, G.; Zhu, C. R.; Han, W. P.; Lu, Y.; Tan, P. H.; Amand, T.; Liu, B. L. et al. Robust optical emission polarization in MoS_2 monolayers through selective valley excitation. *Phys. Rev. B* **2012**, *86*, 081301.

(80) Mak, K. F.; He, K.; Shan, J.; Heinz, T. F. Control of valley polarization in monolayer MoS_2 by optical helicity. *Nature Nanotechnology* **2012**, *7*, 494–498.

(81) Xiao, D.; Liu, G.-B.; Feng, W.; Xu, X.; Yao, W. Coupled Spin and Valley Physics in Monolayers of MoS_2 and Other Group-VI Dichalcogenides. *Phys. Rev. Lett.* **2012**, *108*, 196802.

(82) Singh, S.; Alsharari, A. M.; Ulloa, S. E.; Romero, A. H. *Handbook of Graphene*; John Wiley Sons, Ltd, 2019; Chapter 1, pp 1–28.

(83) Volovik, G. E. Topological Lifshitz transitions. *Low Temperature Physics* **2017**, *43*, 47–55.

(84) Fu, L.; Kane, C. L. Topological insulators with inversion symmetry. *Phys. Rev. B* **2007**, *76*, 045302.

(85) Goedecker, S. Minima hopping: An efficient search method for the global minimum of the potential energy surface of complex molecular systems. *The Journal of Chemical Physics* **2004**, *120*, 9911–9917.

(86) Amsler, M.; Goedecker, S. Crystal structure prediction using the minima hopping method. *The Journal of Chemical Physics* **2010**, *133*, 224104.

(87) Roy, S.; Goedecker, S.; Field, M. J.; Penev, E. A Minima Hopping Study of All-Atom Protein Folding and Structure Prediction. *J. Phys. Chem. B* **2009**, *113*, 7315–7321.

(88) Jensen, F. *Introduction to Computational Chemistry*; Wiley, England, 1998.

(89) Amsler, M. K. Crystal structure prediction based on density functional theory. Ph.D. thesis, University of Basel, 2014.

(90) Pavlic, O.; Ibarra-Hernandez, W.; Valencia-Jaime, I.; Singh, S.; Avendaño-Franco, G.; Raabe, D.; Romero, A. H. Design of Mg alloys: The effects of Li concentration on the structure and elastic properties in the Mg-Li binary system by first principles calculations. *Journal of Alloys and Compounds* **2017**, *691*, 15 – 25.

(91) Singh, S. K. Structural Prediction and Theoretical Characterization of Bi-Sb Binaries: Spin-Orbit Coupling Effects. Ph.D. thesis, West Virginia University, 2018.

(92) Kresse, G.; Joubert, D. From ultrasoft pseudopotentials to the projector augmented-wave method. *Phys. Rev. B* **1999**, *59*, 1758–1775.

(93) Perdew, J. P.; Burke, K.; Ernzerhof, M. Generalized Gradient Approximation Made Simple. *Phys. Rev. Lett.* **1996**, *77*, 3865–3868.

(94) Togo, A.; Tanaka, I. First principles phonon calculations in materials science. *Scr. Mater.* **2015**, *108*, 1–5.

(95) Wu, Q.; Zhang, S.; Song, H.-F.; Troyer, M.; Soluyanov, A. A. WannierTools: An open-source software package for novel topological materials. *Comput. Phys. Commun.* **2018**, *224*, 405 – 416.

Figures

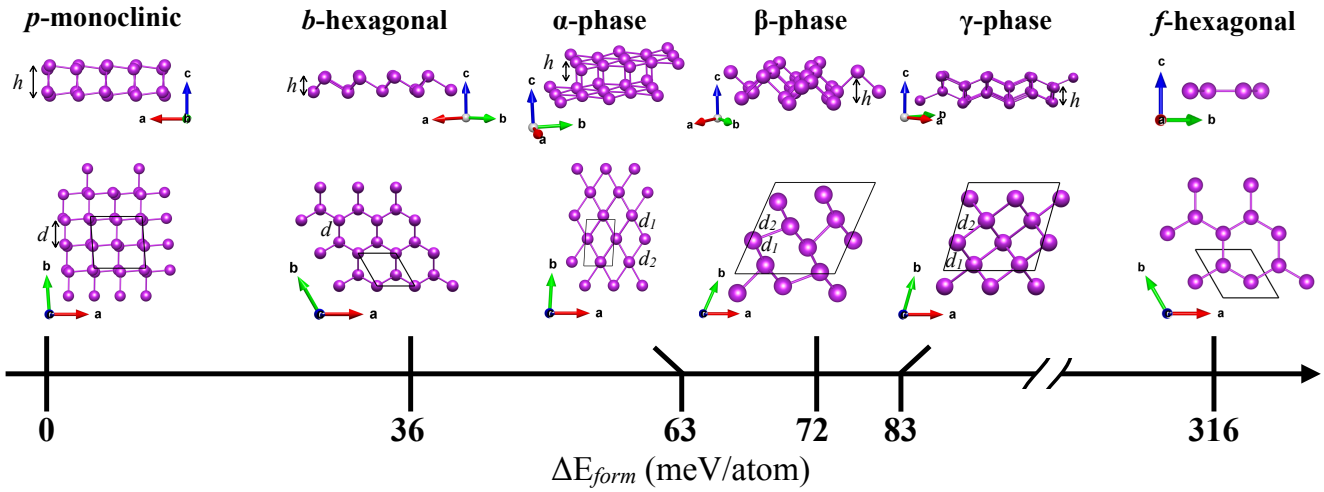

Figure 1: (Color online) Energetic ordering and relaxed structures (side and top views) of the five low-energy phases of monolayer Bi obtained from the cMHM calculations, and one (f-hexa) phase obtained from Ref.[28] The energy differences between phases are given relative to the formation energy of the p-mono phase. Note that the f-hexa phase is 316 meV/atom above the energy of the reference p-mono phase.

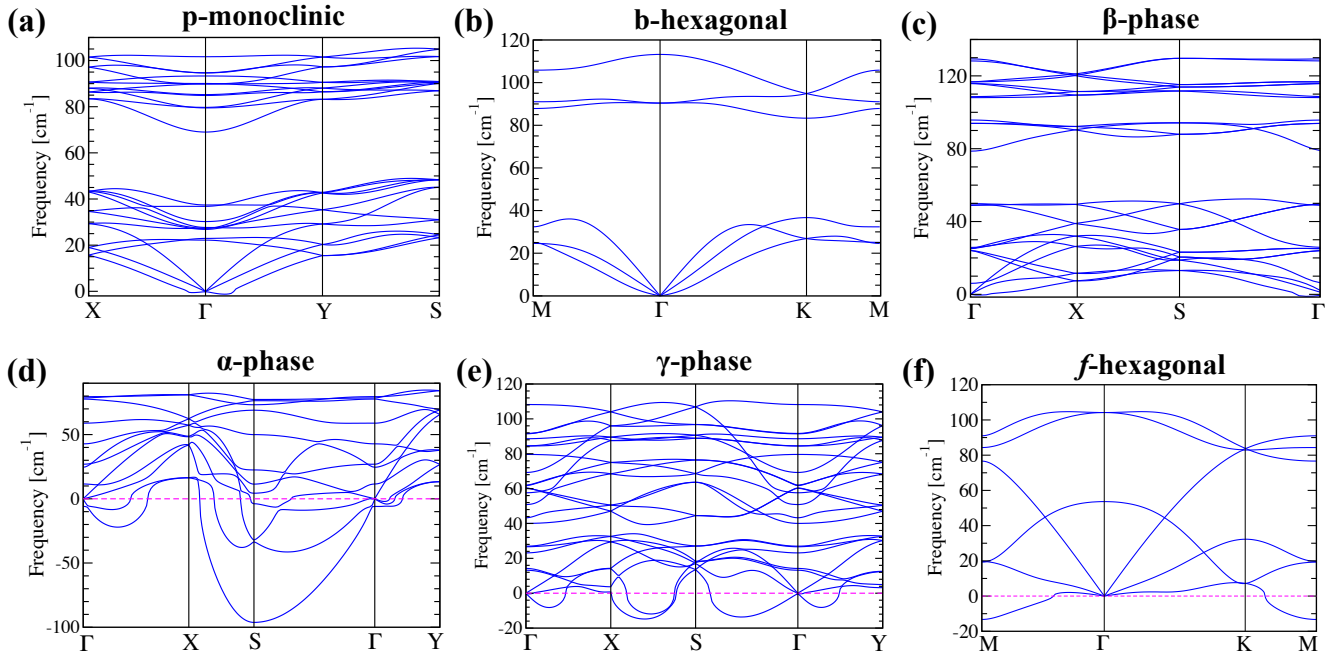

Figure 2: (Color online) Monolayer phonons calculated along the high-symmetry directions in momentum space. The α phase slightly breaks the acoustic sum rule due to numerical differences between the cMHM and PHONOPY calculations.

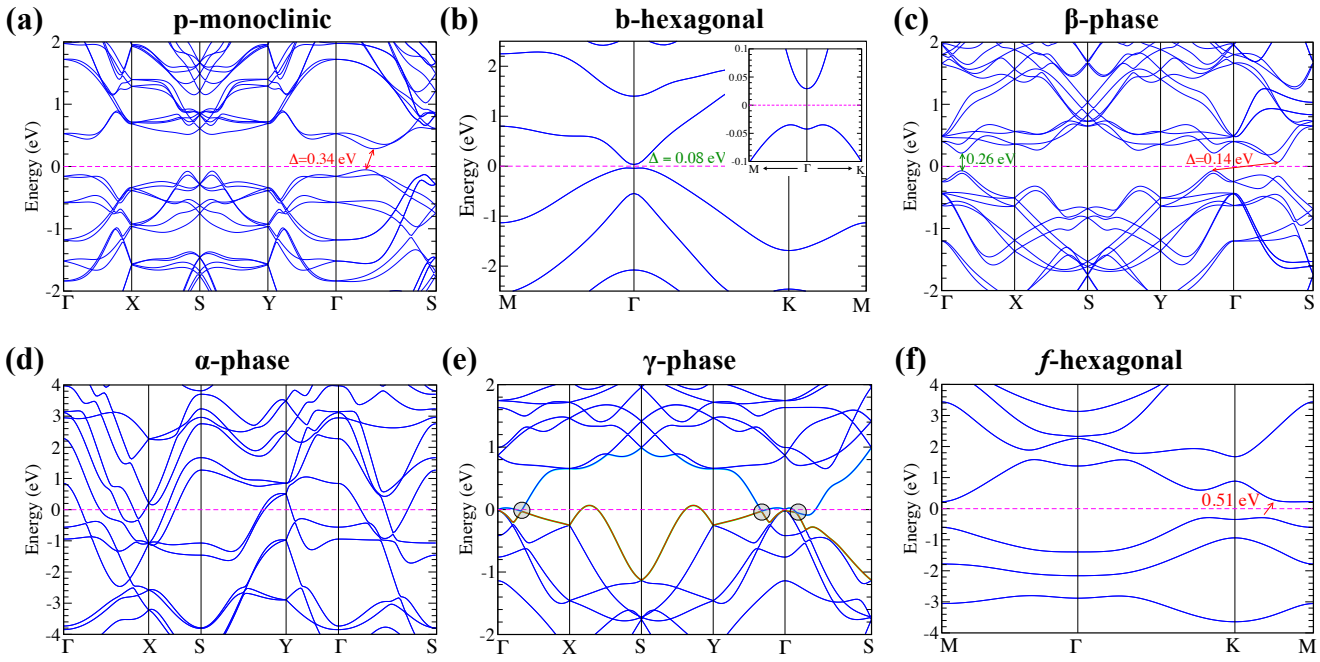

Figure 3: (Color online) Electronic bandstructure calculated with inclusion of SOC for Bi monolayers (see the SM[63] for bandstructure without-SOC). Dashed magenta lines indicate the Fermi-level and Δ denotes energy bandgap in the semiconducting monolayers. The value of direct and indirect gaps are indicated in green and red, respectively. Light colors highlight the spin-degeneracy of bands near the Fermi-level, and circles mark the Dirac points in (e).

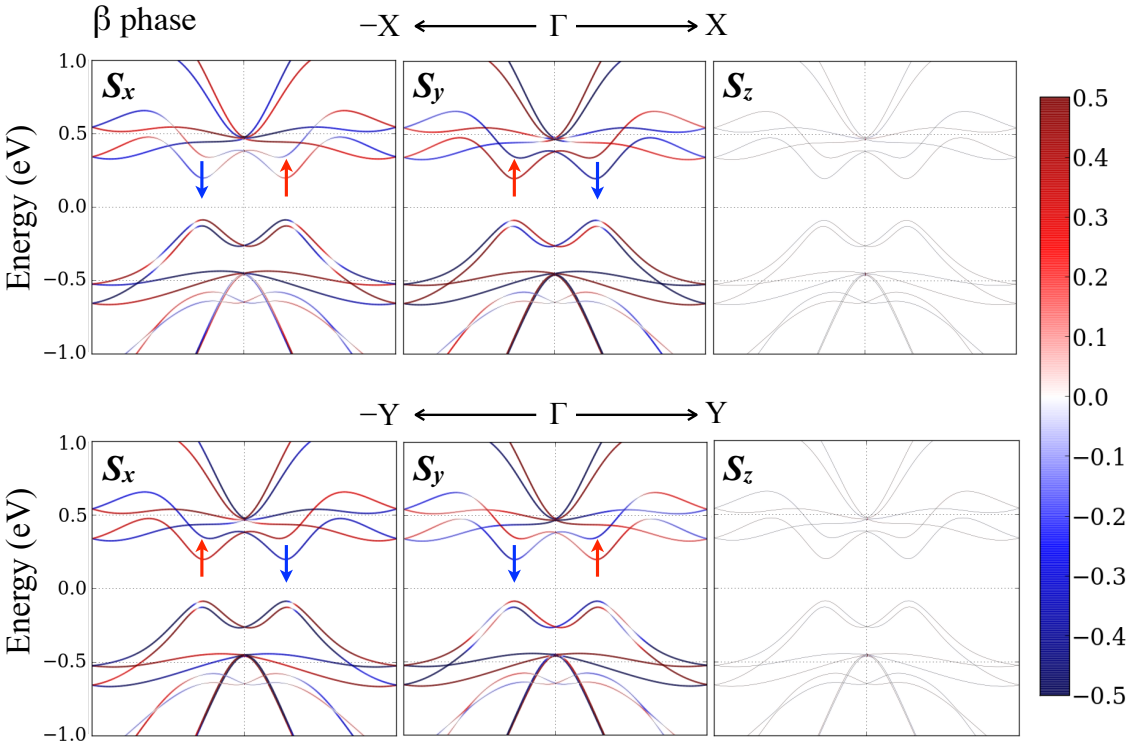

Figure 4: (Color online) Spin projected electronic band structure for β phase. Red/Blue color depicts spin up/down states.

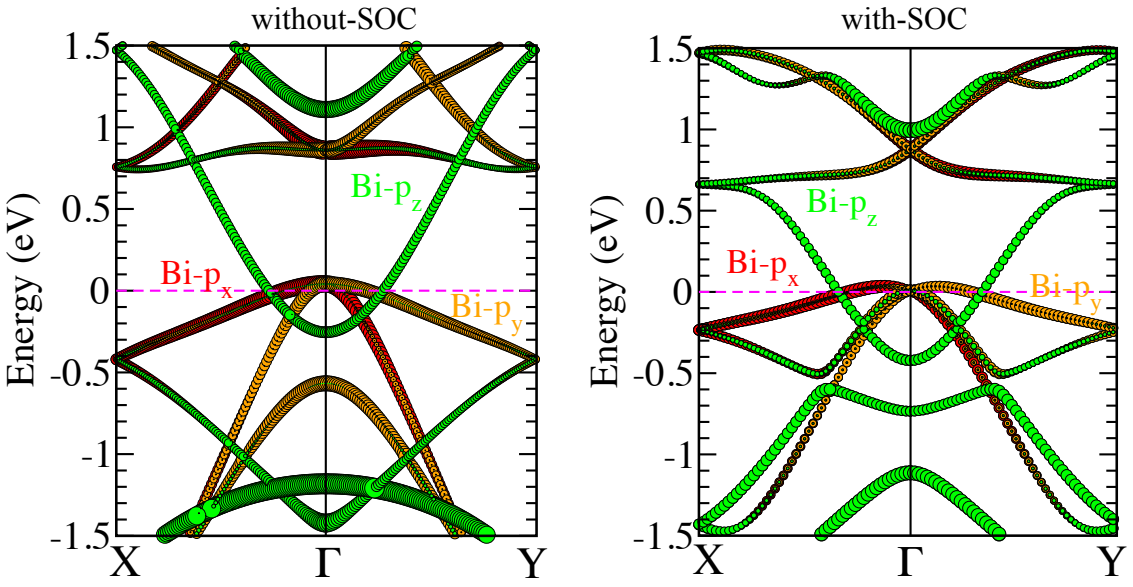

Figure 5: (Color online) Atomic orbital projected electronic band structure of γ phase calculated without-SOC (left panel) and with-SOC (right panel).

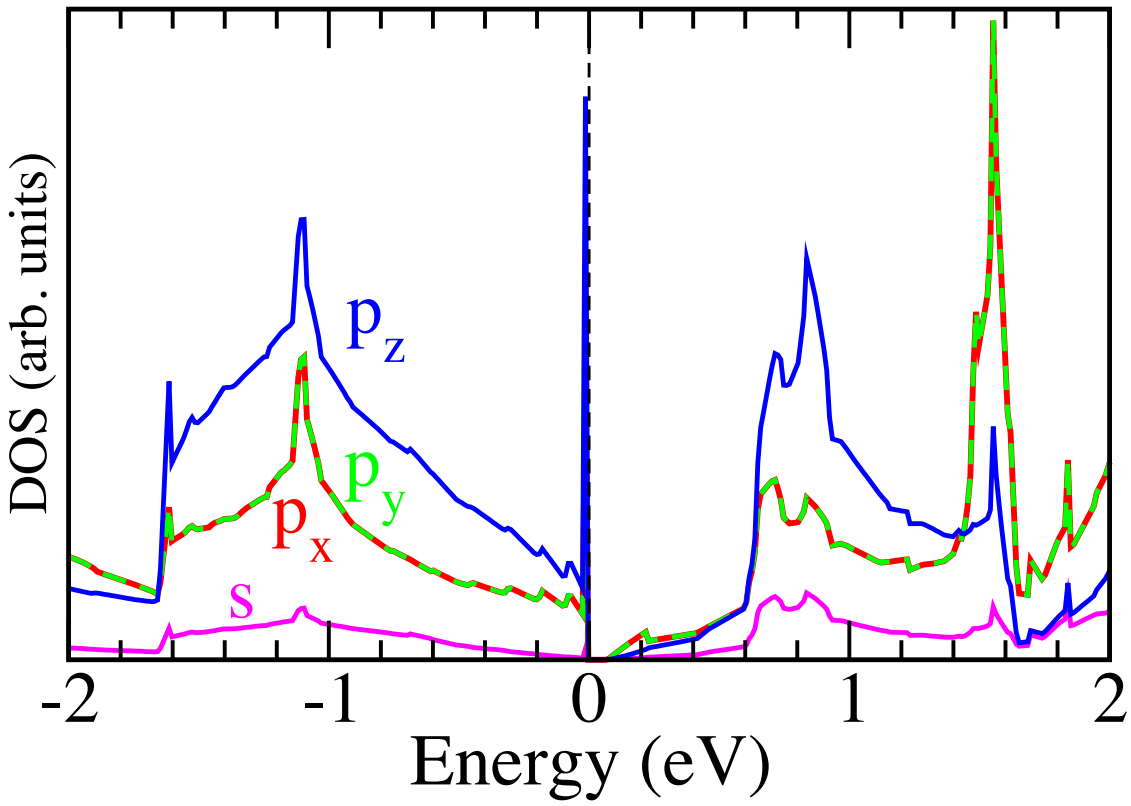

Figure 6: (Color online) Atomic orbitals resolved density of states calculated with-SOC using a k-mesh of size $21 \times 21 \times 1$ for b-hexa phase.